Front. Chem. Sci. Eng. 2023, 17(7): 840−852
https://doi.org/10.1007/s11705-022-2253-0

RESEARCH ARTICLE

Fabrication of recyclable Fe^{3+} chelated aminated polypropylene fiber for efficient clean-up of phosphate wastewater

Shangyuan Zhao[1,2*], Fangjia Wang[3*], Rui Zhou[1,2], Peisen Liu[1,2], Qizhong Xiong[1,2], Weifeng Zhang[1,2], Chaochun Zhang[1,2], Gang Xu (✉)[1,2], Xinxin Ye[1,2], Hongjian Gao[1,2]

1 Anhui Province Key Laboratory of Farmland Ecological Conservation and Pollution Prevention; Engineering and Technology Research Center of Intelligent Manufacture and Efficient Utilization of Green Phosphorus Fertilizer of Anhui Province, College of Resources and Environment, Anhui Agricultural University, Hefei 230036, China
2 Key Laboratory of JiangHuai Arable Land Resources Protection and Eco-restoration, Ministry of Natural Resources, College of Resources and Environment, Anhui Agricultural University, Hefei 230036, China
3 Institute of Soil Science, Chinese Academy of Sciences, Nanjing 210008, China

Abstract Herein, a Fe^{3+}-loaded aminated polypropylene fiber has been reported as an efficient phosphate adsorbent. The remarkable phosphate removal ability of the fiber is due to Fe^{3+} immobilization, and it demonstrates a maximum adsorption capacity of 33.94 mg·P·g^{-1}. Adsorption experiments showed that the fiber is applicable over a wide pH range from 2 to 9. Furthermore, the adsorption kinetics and isotherm data were consistent with the pseudo-second-order and Langmuir adsorption models, respectively. The adsorption equilibrium of the fiber for phosphate was reached within 60 min, indicating an efficient monolayer chemisorption process. Moreover, the adsorbent maintained prominent phosphate removal in the presence of competitive ions such as NO_3^- and Cl^-, exhibiting high selectivity. More importantly, the fiber demonstrated excellent reusability (5 times) and low adsorption limit below 0.02 mg·P·g^{-1}. In addition, the phosphate removal efficiency of the fiber can exceed 99% under continuous flow conditions. The adsorption mechanism was studied by X-ray photoelectron spectroscopy, showing that the adsorption of phosphate on the fiber mainly depended on the chemical adsorption of the modified Fe^{3+}. Overall, this study proves that the fiber possesses many advantages for phosphate removal, including high adsorption efficiency, lower treatment limit, good recyclability, and environmental friendliness.

Keywords phosphate adsorption, aminated polypropylene fiber, Fe^{3+}, ligand exchange, reusability

Received June 24, 2022; accepted September 8, 2022

E-mail: gangxu@ahau.edu.cn

* These authors contributed equally to this work.

1 Introduction

Phosphorus is an important non-renewable resource that is widely used in modern agriculture and in the chemical industry. Presently, phosphate reserves are of low quality and expensive to extract [1]. Furthermore, phosphorus enters the water environment through different routes during various application processes, causing loss of phosphorus resources and water eutrophication [2]. Naturally, phosphorus has diverse chemical forms in water, with phosphate as the main form, leading to water eutrophication. Currently, phosphorus is the limiting factor for water eutrophication, and pollution control in water has always been a global concern. Therefore, considering the economic and environmental benefits, the removal as well as recovery of phosphate from wastewater is of great significance.

To date, several techniques, such as chemical precipitation [3], membrane separation process [4], biological treatment [5], anion exchange [6], and adsorption [7] have been used to remove phosphate. Among them, the adsorption method demonstrates several advantages, such as high efficiency and convenient application, attracting the attention of many researchers. Diverse adsorption materials, such as natural minerals [8], activated carbon [9], and composite materials [10] exist. However, phosphate adsorbents in powder form are difficult to recover in water, which may cause secondary pollution problem, and some materials have the problems of harsh

preparation conditions, high cost, and low removal ability. The preparation of new adsorbents by loading functional groups with specific affinity for phosphate on solid supports can overcome the aforementioned defects, which is one of the research hotspots in recent years [11]. Many researchers have used different metals, metal oxides, and their modified adsorbents for phosphate removal [12–14]. Among the different metals, iron ions have attracted much attention because of their low price, strong binding force with phosphorus, and several sources [15]. In recent years, significant progress has been made in the use of adsorbents, such as iron-modified biochar [16], chitosan [17], zeolite [18], metal organic framework [19], resins [20] and polymers [21] in phosphate removal. However, some of these supports have the disadvantages of difficult recovery, complex preparation, and poor repeatability. Hence, it is important to develop a support material to load iron for phosphate removal with a better performance.

Recently, textile fiber has attracted wide attention as a support material because of its ease of modification, chemical stability, and low cost [22–24]. Compared with other supports, the fibers are flexible and easy to weave, making them applicable to filtering devices in different scenarios [25–27]. Many researchers have successfully constructed functionalized fiber adsorbents for dyes, heavy metals, and phosphate removal, and the results demonstrate that these functionalized fibers have excellent recycling ability and high selectivity for pollutants [28–32]. Furthermore, polypropylene fiber (PPF) demonstrates more acid−alkali resistance, higher mechanical strength, and lower density, making it significant in the field of catalysis and adsorption [33–35]. For example, Zhang et al. [34] prepared alkylbenzene functionalized polypropylene to increase the removal ability of dioctyl phthalate, which demonstrated a high adsorption capacity of 272.4 $mg \cdot g^{-1}$. Li et al. [25] constructed an ion-imprinted PPF for the selective removal of Cu^{2+}, retaining almost the same adsorption capacity even after 10 cycles. Shi et al. [36] reported an ionic liquid-supported PPF for the conversion of fructose to 5-hydroxymethylfurfural with superior catalytic activity and excellent reusability of 10 times. However, the application of functionalized PPF in the purification and recovery of phosphate from water has rarely been reported. Furthermore, textile fibers have dual attributes of resources and pollution. The textile industry is the second-largest source of industrial pollution, accounting for 10% of global carbon emissions [37]. China is the largest fiber consumer with an annual output of approximately 26.1 million tons [38]. The unreasonable utilization of textile fibers causes serious waste of resources and environmental pollution. Therefore, the preparation of phosphate adsorption materials using textile fiber waste has high innovation and practical application value [39].

In this study, PPF was used as a support material to synthesize a novel Fe^{3+}-supported functionalized fiber. First, the amide polypropylene fiber ($PP_{AM}F$) was obtained by a free radical polyreaction between PPF and acrylamide (AM), and ammoniated fiber ($PP_{AMA}F$) was obtained by an amine exchange reaction with hyperbranched polyethylene imine (HPEI). Finally, the $PP_{AMA}F$-Fe was formed by chelating Fe^{3+} on the ammoniated fiber. $PP_{AMA}F$-Fe was systematically characterized to confirm its successful preparation. The phosphate removal ability of the $PP_{AMA}F$-Fe was examined in detail. For example, different influencing factors, such as fiber modification degree, pH of the solution (wastewater), contact temperature, and coexisting anions, were studied for the removal of phosphate by the $PP_{AMA}F$-Fe. Moreover, the adsorption kinetics, isotherms, and thermodynamic models were utilized to illustrate the phosphate adsorption mechanism of $PP_{AMA}F$-Fe. Furthermore, the recycling performance and phosphate removal ability of the $PP_{AMA}F$-Fe in actual wastewater were studied to determine its practical application. Additionally, a continuous flow installation was attempted to remove phosphate using $PP_{AMA}F$-Fe in wastewater.

2 Experimental

2.1 Synthesis of $PP_{AMA}F$-Fe

Three-steps mechanism for $PP_{AMA}F$-Fe synthesis (Fig. S1, cf. Electronic Supplementary Material, ESM): (Step 1) Dried PP (1.0 g), AM (10.0 g), benzoyl peroxide (BPO, 0.03 g), toluene (5.0 g), $(NH_4)_2Fe(SO_4)_2 \cdot 6H_2O$ (0.08 g), and deionized water (20 mL) were mixed in a reaction kettle, and the reaction temperature was set to 85 °C for 1.5 h. After the reaction, the prepared fibers were repeatedly rinsed with water (70–80 °C). Subsequently, an amide fiber ($PP_{AM}F$) with a weight of 17.66% was obtained by drying in an oven at 60 °C overnight. (Step 2) The dried $PP_{AM}F$ (0.2 g) and HPEI (2.0 g) were placed in a reaction kettle with 15 mL H_2O at 110 °C for 6 h. As in the previous step, after cooling, the fibers were washed and dried, and $PP_{AMA}F$ with a weight gain of 13.5% were obtained. $PP_{AMA}F$ with different degrees of modification was obtained by changing the amount of HPEI, more details are provided in Table S1 (cf. ESM). (Step 3) The dried $PP_{AMA}F$ (100 mg) and 50 mL $FeCl_3$ ($0.1\ mol \cdot L^{-1}$) were subjected to a chelation reaction at room temperature. After 2 h of reaction, the fiber with attached Fe^{3+} was rinsed with deionized H_2O. After drying the fiber at 60 °C overnight, Fe^{3+}-supported aminated polypropylene fibers were obtained.

2.2 General procedures of phosphate removal by the functionalized fiber

In a series of adsorption experiments, phosphate

adsorption capability of $PP_{AMA}F$-Fe was measured by setting different solution pH value, temperature, adsorption time and phosphate concentration. When the adsorption reaction ends, the functionalized fiber was taken out from the adsorption system using tweezers, the remained phosphate concentration was determined at the wavelength of 700 nm of Vis spectrophotometer. All adsorption experiments will be conducted parallelly three times, the average value and standard deviation of the adsorption data were calculated.

The pH of KH_2PO_4 sample was adjusted to 3–9 with hydrochloric acid and sodium hydroxide. Then the 10 mg dried $PP_{AMA}F$-Fe were added to 15 mL of KH_2PO_4 (20 mg·P·L^{-1}) solutions of different pH and were stirred by a magnetic stirrer for 1.5 h under room temperature (25 °C).

Adsorption kinetics and adsorption thermodynamic were implemented with 15 mL of phosphate (20 mg·P·L^{-1}) with pH of 6. Different 10 mg dried $PP_{AMA}F$-Fe were added to the solution at different contact temperatures (288, 298 and 308 K). After the above mixed liquid was stirred for 2, 5, 10, 15, 30, 60, 90, 120, 150 and 180 min, the remained phosphate concentration was determined.

At 298 K and pH 6, $PP_{AMA}F$-Fe was immersed into 15 mL of KH_2PO_4 with different original concentration (1–50 mg·P·L^{-1}). After the adsorption equilibrium, the remained phosphate concentration was determined.

In order to reveal the effects of coexisting ion on phosphate adsorption. The Cl^-, NO_3^-, CO_3^{2-} and SO_4^{2-} solutions were prepared with the same initial concentrations (1 mmol·L^{-1}). Then the above anion solution was mixed with identical concentration KH_2PO_4 solution of 1 mmol·L^{-1}, respectively. Then 10 mg dried $PP_{AMA}F$-Fe was immersed into the coexisting ionic solution (15 mL) with electromagnetic stirring for 1.5 h at 25 °C.

Equilibrium adsorption ability (q_e, mg·P·g^{-1}) of $PP_{AMA}F$-Fe, the adsorption capacity at a specific time (q_t, mg·P·g^{-1}), the desorption efficiency (R, %) of $PP_{AMA}F$-Fe-P (phosphate adsorbed by $PP_{AMA}F$-Fe) are calculated as follows:

$$q_e = \frac{(C_o - C_e) \times V}{m}, \tag{1}$$

$$q_t = \frac{(C_o - C_t) \times V}{m}, \tag{2}$$

$$R = \frac{C_o - C_t}{C_o} \times 100\%, \tag{3}$$

where C_o, C_e, C_t represent the initial concentration (mg·P·L^{-1}), equilibrium concentration (mg·P·L^{-1}) and the phosphate concentration (mg·P·L^{-1}) over a certain time. V (mL) is the solution volume and m is the mass (g) of the $PP_{AMA}F$-Fe.

3 Results and discussion

3.1 The preparation of $PP_{AMA}F$-Fe

The $PP_{AMA}F$-Fe synthesis process is shown in Fig. S1, and the fiber photos are presented in Fig. S2 (cf. ESM). PPF cannot react directly with polyethylenimine because of the lack of functional groups that can react with the amino groups [25]. The polymerization chain of PPF contains a tertiary carbon structure, which can easily generate tertiary carbon radicals; thus, AM can be grafted onto PPF by radical polymerization. In the first step of the grafting reaction, BPO generates free radicals (PhCOO·) catalyzed by Fe^{2+}, which attack the PPF surface to produce tertiary carbon radicals, and the tertiary carbon radicals attack the carbon–carbon double bond (C=C) of AM to cause a polymerization reaction. The number of amide functional groups on $PP_{AM}F$ can be controlled by the dosage of AM, and the weight gain of $PP_{AM}F$ relative to PPF was 17.66% in this study. In the second reaction step, the amide groups on the surface of $PP_{AM}F$ reacted with the polyethylene imine through ammonolysis. Therefore, after the above two-step reaction, the fiber surface was modified with amino functional groups, which can easily chelate with Fe^{3+} to prepare the $PP_{AMA}F$-Fe.

The optimization of the $PP_{AMA}F$-Fe synthesis process mainly includes optimizing the functional degree of ammoniated fibers and the concentration of iron to maximize the phosphate adsorption capacity of the functionalized fibers. In this work, the weight gain of the functionalized fiber was used to calculate the degree of modification [40], and the weight of the $PP_{AMA}F$ increased after the amination reaction, proving that HPEI was actually present on the fiber surface. It is well known that HPEI demonstrates high hydrophilicity, hence, the hydrophilicity of the fiber surface is greatly improved after modification [41]. The hydrophilicity of the fiber was evaluated by the water uptake capacity, as shown in Table S2 (cf. ESM), and the water uptake of $PP_{AMA}F$ (28.93%) was higher than that of PPF (4.74%). Furthermore, the amino functional groups on the fiber surface were favorable for chelating Fe^{3+} [42]. By controlling the concentration of the substrate (HPEI, Fe^{3+}), the ammoniated fibers ($PP_{AMA}F$) with different weight gains and grafted with different iron contents were synthesized.

To select suitable functionalized fibers, the phosphate adsorption capacity of the $PP_{AMA}F$-Fe fibers prepared from $PP_{AMA}F$ was analyzed (Fig. S3, cf. ESM). First, the effect of weight gain of aminated fibers chelated with Fe^{3+} on the adsorption of phosphate was tested. The results are presented in Fig. S3(a); the weight gain of the aminated $PP_{AMA}F$ fiber increases with the phosphate purification capacity of $PP_{AMA}F$-Fe. When the weight

gain of $PP_{AMA}F$ was greater than 13.5%, the adsorption capacity of $PP_{AMA}F$-Fe for phosphate remained unchanged. This is because the chelation of Fe^{3+} occurred on the fiber surface, when the weight gain of $PP_{AMA}F$ exceeded a certain value, the amino group was grafted inside the fiber skeleton and could not chelate Fe^{3+} [43]. In addition, a larger degree of modification could also destroy the structure of the fiber surface layer, thus affecting the adsorption capacity [44]. Therefore, a weight gain of 13.5% for $PP_{AMA}F$ was selected.

To verify the role of Fe^{3+} modification, $PP_{AMA}F$ chelated with different Fe^{3+} contents for phosphate removal was investigated. As demonstrated in Fig. S3(b), when compared with $PP_{AMA}F$, the phosphate adsorption ability of $PP_{AMA}F$-Fe evidently improved, proving that Fe^{3+} modification contributes positively to phosphate adsorption. Furthermore, when the initial concentration of Fe ion was higher than 0.1 $mol \cdot L^{-1}$, the phosphate removal ability of $PP_{AMA}F$-Fe attained equilibrium, that is, the chelating ability of $PP_{AMA}F$ to Fe^{3+} reached saturation. Therefore, 100 mg $PP_{AMA}F$ chelated with 50 mL of Fe ion (0.1 $mol \cdot L^{-1}$) was selected as the best synthesis condition for $PP_{AMA}F$-Fe. In this study, $PP_{AMA}F$-Fe was characterized and applied under this optimal condition.

3.2 Characterization of the prepared fibers

3.2.1 Scanning electron microscope (SEM)

Figure 1 depicts the SEM images of the original PPF, $PP_{AM}F$, $PP_{AMA}F$, $PP_{AMA}F$-Fe, and $PP_{AMA}F$-Fe-P fibers. All fibers were continuous and complete when the image was magnified 200 times, indicating that the fiber structure was well maintained. When the SEM of the fibers was magnified by 2000 times, the surface of the

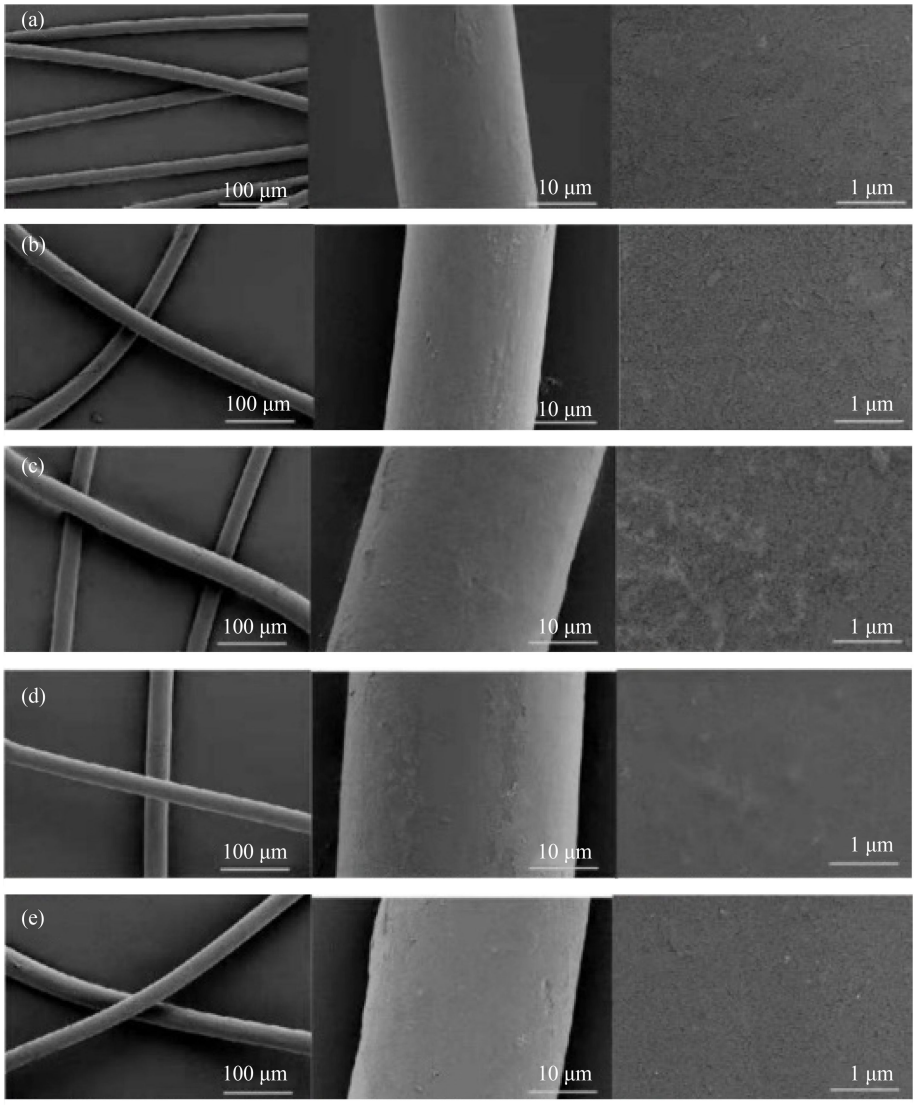

Fig. 1 SEM images of (a) PPF, (b) $PP_{AM}F$, (c) $PP_{AMA}F$, (d) $PP_{AMA}F$-Fe, and (e) $PP_{AMA}F$-Fe-P; the image is magnified 200, 2000, and 20000 times.

functionalized fiber (Figs. 1(c) and 1(d)) was slightly rougher than that before modification, which may be related to the grafting of the monomer to the fiber surface [45]. The diameter expansion of the fibers (Figs. 1(c) and 1(d)) was due to swelling during the reaction process [46]. A crack appeared on the fiber surface (Figs. 1(a–c)) under high magnification (20000 times), which could be beneficial for phosphate adsorption owing to the increase in contact area [25]. After the adsorption of phosphate, the surface of $PP_{AMA}F$-Fe-P (Fig. 1(e)) demonstrated no obvious damage. The results illustrate that the fiber possessed a good structure after use.

3.2.2 Fourier transform infrared spectroscopy (FTIR)

The PPF and functionalized fibers were characterized using FTIR, and the results are presented in Fig. 2. Typical peaks of PPFs (Fig. 2(a)) were concentrated at 1630–1654, 997, and 840 cm^{-1}. The characteristic absorption bands of –C–H for anti-symmetric $–CH_3$, anti-symmetric $–CH_2$, and symmetric $–CH_2$ were observed at 2958, 2920, and 2838 cm^{-1}, respectively [47]. The functionalized fibers exhibited –C=O tensile bands in the 1630–1654 cm^{-1} region, demonstrating the successful grafting of AM onto the fiber (Fig. 2(b)). Furthermore, the wide peak concentrated at 3431 cm^{-1} corresponds to the –N–H asymmetric stretching mode of amine, indicating that HPEI was present on the fiber surface (Fig. 2(c)). After the grafting of Fe^{3+} and the phosphate adsorption (Figs. 2(d) and 2(e)), the peak value and frequency band displacement changed slightly.

3.2.3 Elemental analysis

The elemental analysis of the samples is shown in Table S3 (cf. ESM). PPF (Table S3, entry 1) possesses 1.46% nitrogen, which is due to the nitrogen-containing surfactant during the production procedure [35]. The N content of $PP_{AM}F$ (Table S3, entry 2) increased significantly compared with that of PPF (Table S3, entry 1) because of the introduction of amide N (19.7%). Furthermore, the C content of $PP_{AMA}F$ (Table S3, entry 3) decreased and the N content increased because the C content of HPEI $(C_2H_5N)_n$ (55.81%) was lower than that of $PP_{AM}F$ (74.23%). Similarly, the N content of HPEI (11.63%) is higher than that of $PP_{AM}F$ (6.33%). Moreover, the N, C, and H contents of $PP_{AMA}F$-Fe and $PP_{AMA}F$-Fe-P were reduced (Table S3, entries 4–5), which may be attributed to the introduction of Fe and P. The elemental analysis results indicate that the changes in the content of various elements in the modification process of the fiber are in line with expectations, proving the successful preparation of $PP_{AMA}F$-Fe-P.

3.2.4 X-ray diffraction spectroscopy (XRD)

The crystal structure of the fiber was characterized by XRD (Fig. 3). As shown in Fig. 3(a), the 2θ values of the original PPF were 14°, 16°, 17°, and 18° [48]. The results demonstrate that PPF possessed many crystal line types. After chemical grafting, $PP_{AM}F$, $PP_{AMA}F$, and $PP_{AMA}F$-Fe demonstrated characteristic peaks similar to those of PPF, indicating that the fiber structure remained intact after modification. Some peaks of pure PPF were slightly shifted, showing successful amination versus iron grafting process (Figs. 3(b–d)). Moreover, $PP_{AMA}F$-Fe-P retained its excellent crystal structure after adsorption (Fig. 3(e)). A series of results showed that $PP_{AMA}F$-Fe has high structural stability.

3.3 Effect of pH

The pH of the solution is an important external factor affecting the phosphate removal ability of the functionalized fiber because the pH affects the form of phosphate protons and the surface structure of the fibers simultaneously. Hence, the adsorption capacity of $PP_{AMA}F$-Fe in solutions over a wide pH range of 2–9 was

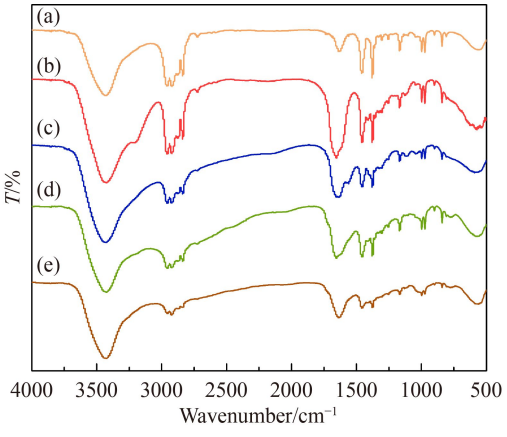

Fig. 2 FTIR spectra of (a) PPF, (b) $PP_{AM}F$, (c) $PP_{AMA}F$, (d) $PP_{AMA}F$-Fe, and (e) $PP_{AMA}F$-Fe-P.

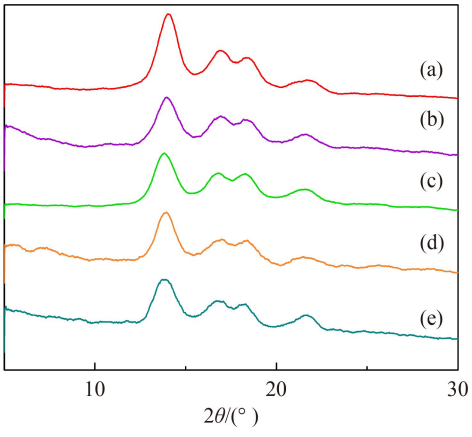

Fig. 3 XRD images of (a) PPF, (b) $PP_{AM}F$, (c) $PP_{AMA}F$, (d) $PP_{AMA}F$-Fe, and (e) $PP_{AMA}F$-Fe-P.

investigated (Fig. 4). The phosphate adsorption capacity of $PP_{AMA}F$-Fe increased gradually between pH 2 and 6, reached the maximum level at pH 6, and then decreased as the pH increased. Furthermore, adsorption is mainly related to the morphology of phosphate and the charge characteristics of the functional groups on the adsorbent [41]. H_3PO_4 is the primary form when the pH of the phosphate solution is lower than 2, which is difficult to bind to Fe^{3+} [42]; therefore, the adsorption capacity is low. At pH values greater than 6, there is competition between OH^-, PO_4^{3-}, and HPO_4^{2-}, which further reduces phosphate adsorption. When the pH was approximately 6, $H_2PO_4^-$ and HPO_4^{2-} were the main forms of phosphate [49], which could easily be combined with Fe^{3+} sites to achieve the best adsorption effect. As the pH between natural water and wastewater is mostly between 5 and 7, $PP_{AMA}F$-Fe demonstrated high phosphate removal capacity in the range of pH 5–7 and possessed optimal removal at pH 6, indicating that $PP_{AMA}F$-Fe has good practical application ability.

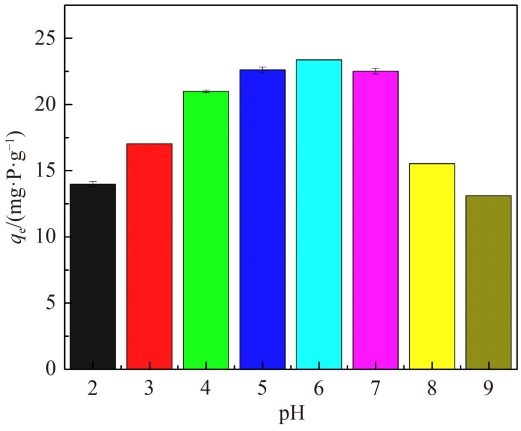

Fig. 4 Effect of pH on phosphate adsorption capacity of $PP_{AMA}F$-Fe.

3.4 Adsorption kinetics and adsorption thermodynamics

Contact time and temperature are important factors affecting the adsorption process, and adsorption kinetics can critically reflect the adsorption efficiency of the fiber adsorbent. The adsorption kinetics and thermodynamics of the $PP_{AMA}F$-Fe for phosphate are presented in Fig. 5. Figure 5(a) shows the adsorption kinetics of $PP_{AMA}F$-Fe for phosphate removal at different temperatures (288, 298, and 308 K). $PP_{AMA}F$-Fe reached half its saturation

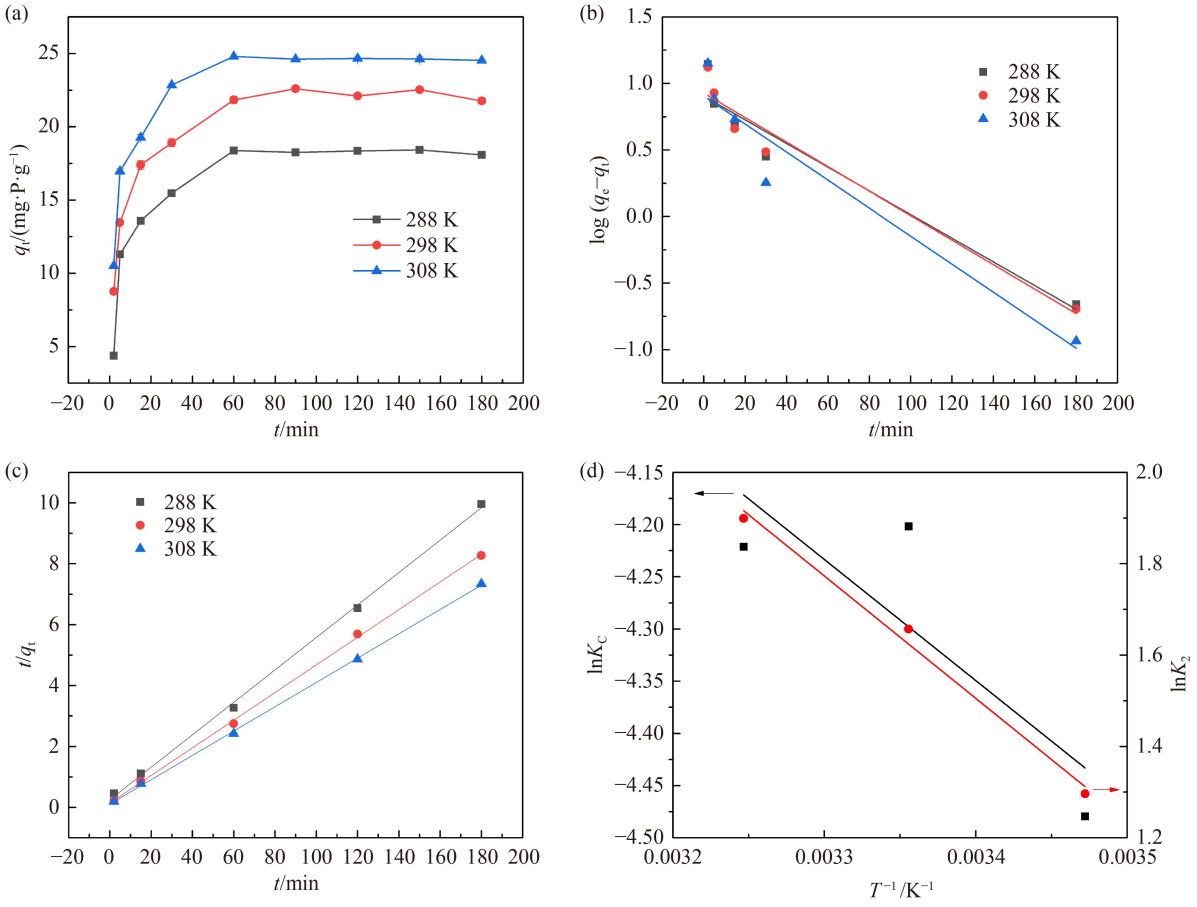

Fig. 5 (a) Phosphate adsorption kinetics of $PP_{AMA}F$-Fe under different temperatures; (b) linear fitting diagram of first-order model; (c) linear fitting diagram of second-order model; (d) the linear equations of lnK_c and 1/T and the linear equations of lnK_2 and 1/T.

level for phosphate in only 5 min, and reached adsorption equilibrium within 60 min, indicating high adsorption efficiency and sensitivity. To better understand the phosphate adsorption by $PP_{AMA}F$-Fe over time, the pseudo-first-order kinetic model (4) and pseudo-second-order kinetic model (5) were applied to fit the phosphate adsorption data. The fitting equations are as follows:

$$\log(q_e - q_t) = \log q_e - \frac{k_1 t}{2.303}, \quad (4)$$

$$\frac{t}{q_t} = \frac{1}{k_2 q_e^2} + \frac{t}{q_e}, \quad (5)$$

where q_t is the removal capacity (mg·P·g^{-1}) at time t, and q_e is the removal capacity (mg·P·g^{-1}) at equilibrium time (min). k_1 and k_2 are the adsorption rate constants. Linear maps of the dynamic pattern are presented in Figs. 5(b) and 5(c), and the adsorption kinetic parameters are listed in Table S4 (cf. ESM). The results confirm that the phosphate adsorption data of $PP_{AMA}F$-Fe were more consistent with the second-order model in terms of the correlation coefficient (Table S4). The first-order kinetic model was found to be in agreement with physical adsorption, while the second-order kinetic model tends to describe chemical adsorption [41], hence the removal of phosphate by $PP_{AMA}F$-Fe is more inclined to the chemisorption mechanism.

The phosphate removal ability of $PP_{AMA}F$-Fe increased (Fig. 5(a)) with an increase in the temperature of the solution, indicating that phosphate removal by $PP_{AMA}F$-Fe is an endothermic process. To better reveal the influence of temperature, some typical thermodynamic parameters, such as Gibbs free energy (ΔG^0, kJ·mol^{-1}), standard enthalpy (ΔH^0, kJ·mol^{-1}), and standard entropy (ΔS^0, kJ·mol^{-1}), were used to provide information on thermodynamic parameters during the adsorption process. The thermodynamic parameters were calculated as follows:

$$K_c = \frac{C_{Ae}}{C_e}, \quad (6)$$

$$\Delta G^o = -RT\ln K_c, \quad (7)$$

$$\ln K_c = \frac{\Delta S^o}{R} - \frac{\Delta H^o}{RT}, \quad (8)$$

where K_c is the distribution coefficient of adsorption, C_{Ae} is the adsorbed phosphate on $PP_{AMA}F$-Fe (mg·P·L^{-1}), R is the ideal gas constant (8.314 J·mol^{-1}·K^{-1}), and T is temperature (K).

Table S5 (cf. ESM) lists the thermodynamic parameters of the functionalized fibers. ΔG^0 with a negative value proves that phosphate removal by $PP_{AMA}F$-Fe is spontaneous, and the greater the absolute value of ΔG^0, the higher the driving force and phosphate adsorption capacity. The positive value of ΔH^0 (9.64 kJ·mol^{-1}) provides evidence for the endothermic reaction of $PP_{AMA}F$-Fe with phosphate. Furthermore, ΔS^0 with a positive value illustrates that the randomness of the system increases during phosphate adsorption process by $PP_{AMA}F$-Fe [34]. In addition, the activation energy E_a = 22.27 kJ·mol^{-1} calculated by the linear equations of $\ln K_2$ and $1/T$ (Fig. 5(d)), further indicating that chemisorption is the dominant adsorption mechanism of phosphate by $PP_{AMA}F$-Fe.

3.5 The effect of phosphate initial concentration

Adsorption isotherms help determine the largest adsorption ability of an adsorbent and explain the principle of adsorption [43]. The phosphate removal ability of $PP_{AMA}F$-Fe at different initial phosphate concentrations was studied at 298 K. As depicted in Fig. 6, the adsorption capacity of $PP_{AMA}F$-Fe increased with increasing initial phosphate concentration; at the initial stages of the phosphate concentration increase, the amount of phosphate adsorption increased rapidly until adsorption equilibrium was reached. The maximum phosphate adsorption capacity of $PP_{AMA}F$-Fe was 32.42 mg·P·g^{-1}. This is because a high phosphate concentration improved the recognition and binding of phosphate to Fe^{3+} sites, and the phosphate removal ability

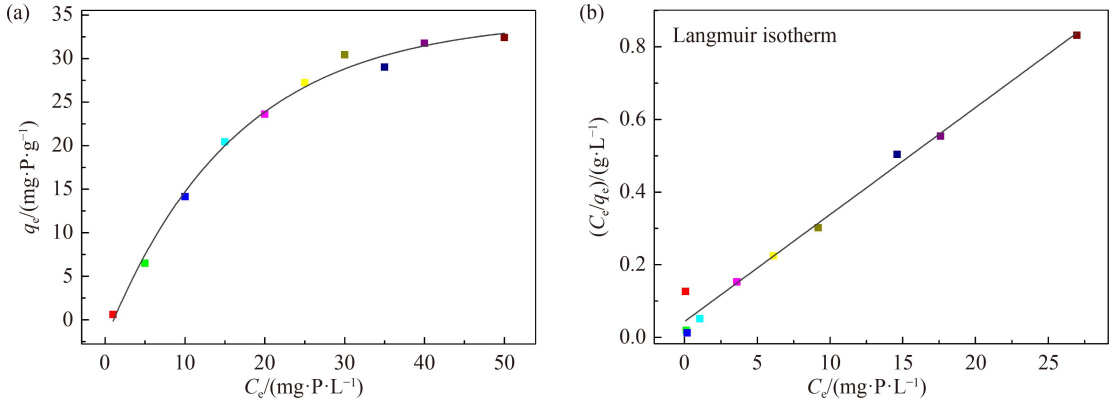

Fig. 6 (a) Effect of phosphate concentrations on the phosphate removal capacity of $PP_{AMA}F$-Fe; (b) linear fitting of the Langmuir isotherm model of $PP_{AMA}F$-Fe for phosphate adsorption.

of the fiber gradually attained saturation with the depletion of Fe^{3+} sites on the fiber surfaces [41].

To better describe and analyze the adsorption isotherms, the most common isotherm models, Langmuir (9) and Freundlich (10), were used. The Langmuir model assumes equal availability of adsorption sites, monolayer surface coverage, adsorption uniformity, and non-interactions between adsorption molecules [50]. Meanwhile, the Freundlich model was used to explain heterogeneous adsorption, which describes reversible adsorption and is not limited to monolayer adsorption [47]. The linearized Langmuir and Freundlich models are as follows:

$$\frac{C_e}{q_e} = \frac{C_e}{q_{max}} + \frac{1}{K_l \times q_{max}}, \quad (9)$$

$$\log q_e = \log K_f + \frac{\log C_e}{n}, \quad (10)$$

where q_{max} (mg·P·g^{-1}) is the maximum adsorption capacity and K_l (L·g^{-1}) and K_f (mg·g^{-1}) are the Langmuir and Freundlich adsorption constants, respectively. By fitting the two models to the experimental data, Figs. 6(b) and S4 (cf. ESM) were obtained, and the corresponding coefficients are listed in Table S6 (cf. ESM).

Comparing the Langmuir isotherm model (R^2 = 0.98266) and Freundlich model (R^2 = 0.82777), the former demonstrates a better linear regression correlation. In other words, the Langmuir isotherms can better describe the equilibrium data. Hence, it can be concluded that the Fe^{3+} responsible for phosphate adsorption is uniformly distributed on the surface of the functionalized fiber, and that the adsorption of phosphate by PP_{AMA}F-Fe is monolayer adsorption on the fiber surface. Theoretically, the maximum removal ability of the PP_{AMA}F-Fe for phosphate is 33.94 mg·P·g^{-1} calculated by the Langmuir isotherm, which is superior to the reported phosphate adsorbent materials, such as Fe(III) loaded chitosan-biochar composite fiber (19.24 mg·P·g^{-1}) [16], crosslinked Fe(III)-chitosan (10.2 mg·P·g^{-1}) [17], and Fe-La/MgO nanosheets (12.28 mg·P·g^{-1}) [51]. Therefore, PP_{AMA}F-Fe is an excellent adsorption material with a high phosphate removal capacity.

3.6 Adsorption selectivity and adsorption limit

Adsorption selectivity or the competitive ion effect is a key factor in evaluating the adsorption ability of adsorbents [52]. To assess the selective removal of phosphate by PP_{AMA}F-Fe in the presence of other anions-coexisting in water bodies, identical concentrations of Cl^-, CO_3^{2-}, NO_3^-, and SO_4^{2-} were added to the phosphate solution (1 mmol·L^{-1}), and the result is shown in Fig. 7. The order of influence of coexisting ions was SO_4^{2-} > CO_3^{2-} > NO_3^- > Cl^-, indicating that Cl^- and NO_3^- had little hindrance to the adsorption of phosphate by PP_{AMA}F-Fe (Fig. 7(a)). However, the CO_3^{2-} and SO_4^{2-} affected the decrease of phosphate adsorption from 21.99 to 6.60 and 5.81 mg·P·g^{-1}, respectively, which may be owing to the strong affinity of the two ions for the Fe^{3+} on PP_{AMA}F-Fe, thus competing with phosphate ions [42]. Despite the influence of the coexisting anions, an adsorption capacity of more than 5 mg·P·g^{-1} was obtained, which proves that PP_{AMA}F-Fe has good adsorption selectivity and highly practical.

To verify the phosphate removal by PP_{AMA}F-Fe in real water, natural lake water (Chaohu Lake) was selected for the phosphate adsorption experiments. The main anions in Chaohu Lake are shown in Table S7 (cf. ESM), which shows that the composition of the water body is complex, and the contents of several anions are higher than that of phosphate. To highlight the practical application of PP_{AMA}F-Fe, the phosphate concentration in the real water was adjusted to 4510 μg·P·L^{-1}. In 15 mL of the above-mentioned water specimen, different qualities of PP_{AMA}F-Fe were magnetically stirred for 24 h; the details are shown in Table S8 (cf. ESM). With a PP_{AMA}F-Fe content of more than 50 mg, the phosphate concentration was reduced to the strictest international standard of a

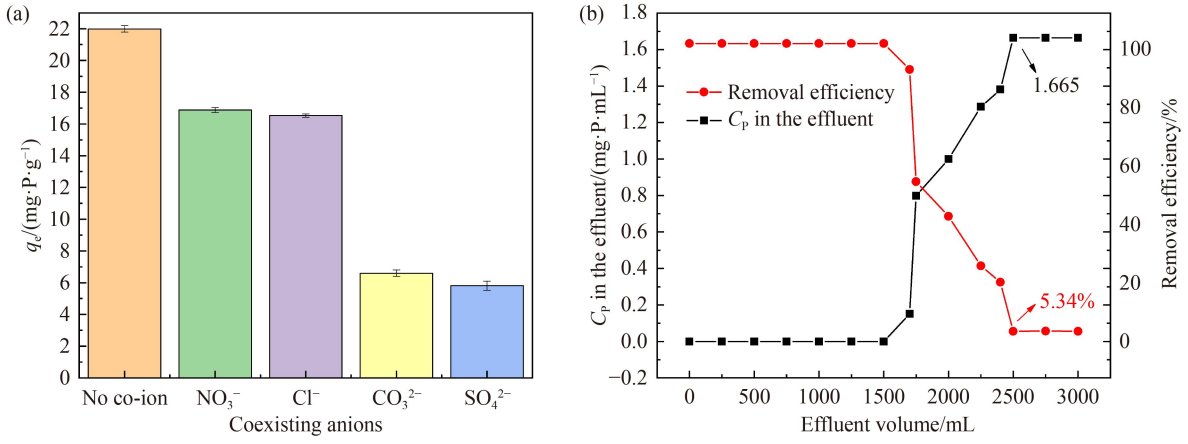

Fig. 7 (a) Phosphate removal ability by PP_{AMA}F-Fe in competitive ions solution; (b) breakthrough curves of phosphate solutions.

maximum concentration of 10 μg·P·L^{-1} required to avoid water eutrophication [53]. Therefore, $PP_{AMA}F$-Fe has good application prospects in the prevention of water bodies eutrophication.

3.7 Application of $PP_{AMA}F$-Fe in continuous flow model

We constructed a flow adsorption model using a silicone tube (100 mm in length and 5.6 mm in diameter) and a peristaltic pump to verify the performance of $PP_{AMA}F$-Fe in removing phosphate under continuous flow conditions. The specific operation was to fill 300 mg $PP_{AMA}F$-Fe into a silicone tube, and then the phosphate solution (2 mg·P·L^{-1}) was injected into the peristaltic pump at a flow rate of 0.8 mL·min^{-1}. Finally, the phosphate concentration in the outflow was measured at intervals to obtain the phosphate breakthrough curve (Fig. 7(b)). The phosphate removal rate was greater than 99% when the outflow liquid product was less than 1700 mL, demonstrating the good removal capacity of $PP_{AMA}F$-Fe under continuous flow conditions. Because of the flexibility and plasticity of the fiber materials, they can be woven into different shapes to match the treatment of various water bodies, showing broad application prospects for $PP_{AMA}F$-Fe.

3.8 Desorption and reusability studies

The reusability of a sorbent material is an important parameter in practical applications. Therefore, the adsorption-desorption process was repeated to evaluate the reusability of $PP_{AMA}F$-Fe. After optimized comparison, 30 mL of 0.1 mol·L^{-1} ethylene diamine triacetic acid (EDTA) was selected as the optimum desorption condition (Table S9, cf. ESM). As displayed in the Fig. S5 (cf. ESM), the phosphate ions on $PP_{AMA}F$-Fe were desorbed by a 0.1 mol·L^{-1} EDTA solution with a desorption rate of 99%. When the adsorption−desorption process was repeated five times, the phosphate removal rate was 99%, indicating that $PP_{AMA}F$-Fe has excellent tolerance and reusability.

3.9 Adsorption mechanism

The phosphate adsorption mechanism of $PP_{AMA}F$-Fe was analyzed using energy dispersive spectroscopy (EDS) and X-ray photoelectron spectroscopy (XPS), the results are described in Fig. 8. The contents and distributions of the elements obtained by EDS are shown in Fig. 8(a) and Table S10 (cf. ESM). The results show that the original PPF contained mainly C. Compared with PPF, new N and O peaks appeared after the two-step amination modification of $PP_{AMA}F$, indicating that amines were successfully grafted onto $PP_{AMA}F$ (Fig. 8(a), traces I–II). Moreover, after chelating Fe^{3+}, new Fe and Cl peaks appeared in the $PP_{AMA}F$-Fe spectrum, revealing that Fe^{3+} was successfully loaded onto the fiber (Fig. 8(a), trace IV). When the adsorption reaction ended, the spectrum of $PP_{AMA}F$-Fe-P showed a new P peak, and the Cl peak decreased (Fig. 8(a), trace V). This phenomenon indicates that $PP_{AMA}F$-Fe can successfully adsorb phosphate, and that the binding between Fe and P is accomplished by ligand exchange between Cl^- and phosphate anions.

XPS characterization of the fibers was performed to prove the phosphate adsorption mechanism of $PP_{AMA}F$-Fe. The spectra and corresponding atomic compositions of the XPS survey are presented in Fig. 8(b) and Table S11 (cf. ESM), respectively. As seen in Fig. 8(b), new element peaks of Fe and Cl were found in $PP_{AMA}F$-Fe, which were similar to the EDS results. These results indicate that $PP_{AMA}F$-Fe was successfully constructed. Furthermore, the high-resolution spectrum of Fe 2p for $PP_{AMA}F$-Fe could be decomposed into $2p_{1/2}$ at 725.536 eV and $2p_{3/2}$ at 711.731 eV (Fig. 8(e)). When the adsorption reaction ended, the binding energy of the Fe 2p peak shifted to 725.531 and 711.915 eV, and the Cl content of $PP_{AMA}F$-Fe-P decreased significantly, illustrating that phosphate and Cl^- ions exchange, and the valence band of Fe 2p may undergo electron transfer and form Fe–O–P bonding to successfully adsorb phosphate [54], which was also demonstrated in a previous study of an iron-modified SMER for phosphate removal [55].

In addition, there were three main types of nitrogen in the high-resolution spectrum of $PP_{AMA}F$-Fe (Fig. 8(f)): amide O≡C–N (401.49 eV), –NH–/–NH_2 (399.83 eV), and tertiary amine –NR_2 (399.13 eV) [30]. The binding energies of the N 1s spectrum increased to 401.60, 399.95 and 399.16 eV separately after the adsorption reaction was terminated, which was caused by the protonation of the amine groups [56]. Protonated amines, such as –NH_3^+, can absorb phosphate ions through electrostatic attraction [57]. By analyzing and summarizing the above, a feasible adsorption mechanism was proposed, as shown in Fig. S6 (cf. ESM). The phosphate adsorption mechanism of $PP_{AMA}F$-Fe may be the coordination reaction between Fe and phosphorus and the electrostatic attraction of protonated amines and phosphate ions.

3.10 Comparison with other iron modified adsorbents for phosphate removal

The maximum adsorption ability, equilibrium time, and repeatability of $PP_{AMA}F$-Fe were compared with those of other reported phosphate adsorbents modified with iron. As shown in Table 1, $PP_{AMA}F$-Fe exhibited a higher phosphate adsorption ability than most reported adsorbents. Furthermore, the adsorption equilibrium time of $PP_{AMA}F$-Fe for phosphate was shorter than that of many other adsorbents; hence, the functionalized fiber showed excellent adsorption sensitivity. Importantly, $PP_{AMA}F$-Fe exhibited excellent performance in removing phosphate efficiently after five cycles. In addition, as a

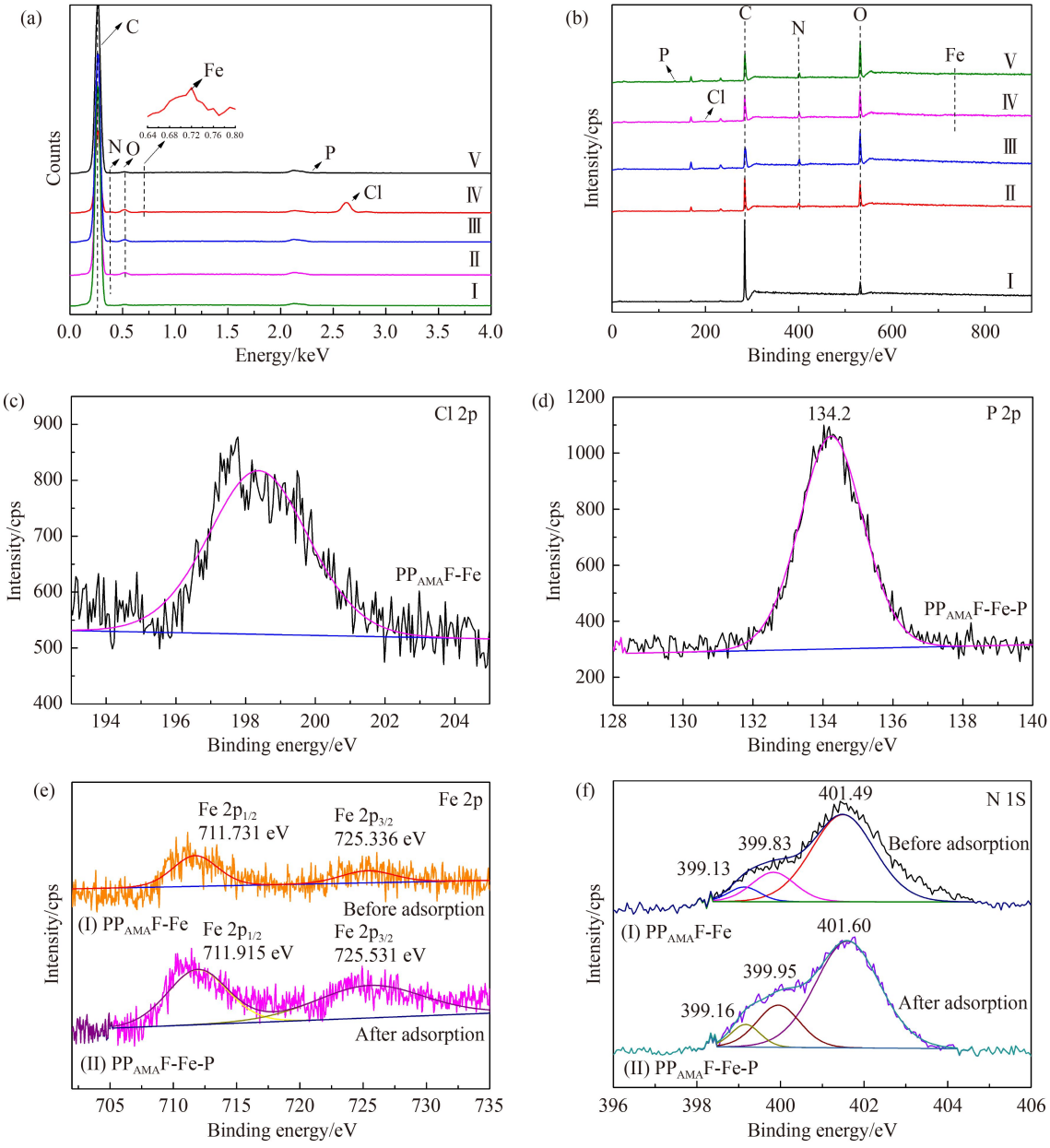

Fig. 8 (a) EDS spectra of (I–V) PPF, $PP_{AM}F$, $PP_{AMA}F$, $PP_{AMA}F$-Fe, and $PP_{AMA}F$-Fe-P; (b) XPS survey of PPF, $PP_{AM}F$, $PP_{AMA}F$, $PP_{AMA}F$-Fe, and $PP_{AMA}F$-Fe-P; (c) high resolution spectrum of Cl 2p for $PP_{AMA}F$-Fe; (d) high resolution spectrum of P 2p for $PP_{AMA}F$-Fe-P; (e) high resolution Fe 2p spectrum of $PP_{AMA}F$-Fe and $PP_{AMA}F$-Fe-P; (f) high resolution N 1s spectrum of $PP_{AMA}F$-Fe and $PP_{AMA}F$-Fe-P.

Table 1 Different iron modified adsorbents for phosphate removal

Adsorbents	q_e/(mg·P·g^{-1})	Equilibrium time	Run	Ref.
Fe(III) loaded chitosan-biochar composite fibers	19.24	240 min	–	[16]
Calcium-modified iron-based adsorbents ($Fe/CaCl_2$)	16.97	20 min	–	[58]
Crosslinked Fe(III)-chitosan (CTS-Fe-CL)	10.20	300 min	5	[17]
Fe(III)-doped chitosan (CTS-Fe)	15.70	300 min	5	[17]
Fe-La/MgO nanosheets	12.28	80 min	–	[51]
Eggshell functionalized with iron oxyhydroxide	21.98	240 min	–	[59]
microporous Fe_2O_3/g-C_3N_4	17.11	15 min	5	[60]
$PP_{AMA}F$-Fe	34.42	60 min	5	This study

very mature synthetic fiber, the cost of commercial PPF is low, and $PP_{AMA}F$-Fe can also be prepared using PPF waste, which provides a new method for the resource utilization of fiber solid waste. Therefore, the removal of phosphate by $PP_{AMA}F$-Fe is highly cost-effective and environmentally friendly. In summary, $PP_{AMA}F$-Fe has the advantages of low cost, low removal limit, high adsorption capacity, excellent recyclability, and environmental friendliness.

4 Conclusions

Phosphorus pollution is a significant bottleneck that restricts water quality safety and has become a topic of global concern. In this study, PPF was used as a support to prepare a novel adsorbent to remove phosphate from wastewater, providing an important approach for the reutilization of fiber waste and the purification of phosphate. First, $PP_{AMA}F$-Fe was developed and optimized via a three-step synthesis process. The phosphate adsorption capacity was significantly enhanced (33.94 $mg \cdot P \cdot g^{-1}$) by the modification of Fe^{3+}. According to the phosphate adsorption experiment, $PP_{AMA}F$-Fe showed wide pH adaptability, with an optimal pH of 6 and high adsorption efficiency within an adsorption equilibrium time of 60 min. Furthermore, $PP_{AMA}F$-Fe exhibited excellent reusability of five times and high selectivity for phosphate in the presence of competing ions such as Cl^- and NO_3^-. In addition, $PP_{AMA}F$-Fe exhibited a prominent removal efficiency of 99% under continuous flow conditions, proving its applicability to flowing water. More importantly, $PP_{AMA}F$-Fe can reduce the phosphate in simulated sewage from 4500 $\mu g \cdot P \cdot L^{-1}$ to below 10 $\mu g \cdot P \cdot L^{-1}$, which is lower than the international standard of minimum P concentration that causes eutrophication. The dynamics and isotherm adsorption data were more consistent with the pseudo-second-order kinetic and Langmuir linear equations, proving that the adsorption mechanism is more inclined toward monolayer chemical adsorption. The thermodynamic parameters indicated that the activation energy of phosphate removal by $PP_{AMA}F$-Fe was 22.27 $kJ \cdot mol^{-1}$, further illustrating a chemisorption process. Furthermore, the XPS proves that the interaction between phosphate and Fe^{3+} is mainly responsible for the adsorption process. In brief, owing to the advantages of the fiber support, $PP_{AMA}F$-Fe exhibited competitive characteristics, including high efficiency, good selectivity, and excellent reusability, as well as economic and environmental benefits.

Acknowledgements This work was financially supported by the National Natural Science Foundation of China (Grant No. 22208003), Natural Science Foundation of Anhui Province (No. 1908085QB87), Major Science and Technology Projects in Anhui Province (No. 202103a06020012).

Electronic Supplementary Material Supplementary material is available in the online version of this article at https://dx.doi.org/10.1007/s11705-022-2253-0 and is accessible for authorized users.

References

1. Cordell D, Drangert J O, White S. The story of phosphorus: global food security and food for thought. Global Environmental Change, 2009, 19(2): 292–305
2. Shahat A, Hassan H M A, Azzazy H M E, Hosni M, Awual M R. Novel nano-conjugate materials for effective arsenic(V) and phosphate capturing in aqueous media. Chemical Engineering Journal, 2018, 331: 54–63
3. Lacson C F Z, Lu M C, Huang Y H. Calcium-based seeded precipitation for simultaneous removal of fluoride and phosphate: its optimization using BBD-RSM and defluoridation mechanism. Journal of Water Process Engineering, 2022, 47: 10265
4. Karthikeyan P, Banu H A T, Meenakshi S. Removal of phosphate and nitrate ions from aqueous solution using La^{3+} incorporated chitosan biopolymeric matrix membrane. International Journal of Biological Macromolecules, 2019, 124: 492–504
5. Sun S, Gao M, Wang Y, Qiu Q, Han J, Qiu L, Feng Y. Phosphate removal via biological process coupling with hydroxyapatite crystallization in alternating anaerobic/aerobic biofilter reactor. Bioresource Technology, 2021, 326: 124728
6. Dong H, Wei L, Tarpeh W A. Electro-assisted regeneration of pH-sensitive ion exchangers for sustainable phosphate removal and recovery. Water Research, 2020, 184: 116167
7. dos Reis G S, Thue P S, Cazacliu B G, Lima E C, Sampaio C H, Quattrone M, Ovsyannikova E, Kruse A, Dotto G L. Effect of concrete carbonation on phosphate removal through adsorption process and its potential application as fertilizer. Journal of Cleaner Production, 2020, 256: 120416
8. Huo J, Min X, Wang Y. Zirconium-modified natural clays for phosphate removal: effect of clay minerals. Environmental Research, 2021, 194: 110685
9. Miyazato T, Nuryono N, Kobune M, Rusdiarso B, Otomo R, Kamiya Y. Phosphate recovery from an aqueous solution through adsorption−desorption cycle over thermally treated activated carbon. Journal of Water Process Engineering, 2020, 36: 101302
10. Awual M R. Efficient phosphate removal from water for controlling eutrophication using novel composite adsorbent. Journal of Cleaner Production, 2019, 228: 1311–1319
11. Awual M R, Jyo A, Ihara T, Seko N, Tamada M, Lim K T. Enhanced trace phosphate removal from water by zirconium(IV) loaded fibrous adsorbent. Water Research, 2011, 45(15): 4592–4600
12. Chen Y, Xu R, Li Y, Liu Y, Wu Y, Chen Y, Zhang J, Chen S, Yin H, Zeng Z, Wang S, Peng Z. $La(OH)_3$-modified magnetic $CoFe_2O_4$ nanocomposites: a novel adsorbent with highly efficient activity and reusability for phosphate removal. Colloids and Surfaces A: Physicochemical and Engineering Aspects, 2020, 599: 124870
13. Jia Z, Zeng W, Xu H, Li S, Peng Y. Adsorption removal and reuse of phosphate from wastewater using a novel adsorbent of

lanthanum-modified platanus biochar. Process Safety and Environmental Protection, 2020, 140: 221–232

14. Liu R, Shen J, He X, Chi L, Wang X. Efficient macroporous adsorbent for phosphate removal based on hydrate aluminum-functionalized melamine sponge. Chemical Engineering Journal, 2021, 421(2): 127848
15. Delgadillo-Velasco L, Hernández-Montoya V, Ramírez-Montoya L A, Montes-Morán M A, del Rosario Moreno-Virgen M, Rangel-Vázquez N A. Removal of phosphate and aluminum from water in single and binary systems using iron-modified carbons. Journal of Molecular Liquids, 2021, 323: 114586
16. Palansooriya K N, Kim S, Igalavithana A D, Hashimoto Y, Choi Y E, Mukhopadhyay R, Sarkar B, Ok Y S. Fe(III) loaded chitosan-biochar composite fibers for the removal of phosphate from water. Journal of Hazardous Materials, 2021, 415: 125464
17. Zhang B, Chen N, Feng C, Zhang Z. Adsorption for phosphate by crosslinked/non-crosslinked-chitosan-Fe(III) complex sorbents: characteristic and mechanism. Chemical Engineering Journal, 2018, 353: 361–372
18. Lu Z, Zhang K, Liu F, Gao X, Zhai Z, Li J, Du L. Simultaneous recovery of ammonium and phosphate from aqueous solutions using Mg/Fe modified NaY zeolite: integration between adsorption and struvite precipitation. Separation and Purification Technology, 2022, 299: 121713
19. Liu M, Huang Q, Li L, Zhu G, Yang X, Wang S. Cerium-doped MIL-101-NH_2(Fe) as superior adsorbent for simultaneous capture of phosphate and As(V) from Yangzonghai coastal spring water. Journal of Hazardous Materials, 2022, 423: 126981
20. Awual M R, Jyo A. Assessing of phosphorus removal by polymeric anion exchangers. Desalination, 2011, 281: 111–117
21. Xu W, Zheng W, Wang F, Xiong Q, Shi X L, Kalkhajeh Y K, Xu G, Gao H. Using iron ion-loaded aminated polyacrylonitrile fiber to efficiently remove wastewater phosphate. Chemical Engineering Journal, 2021, 403: 126349
22. Zheng W, Wu Q, Xu W, Xiong Q, Kianpoor Kalkhajeh Y, Zhang C, Xu G, Zhang W, Ye X, Gao H. Efficient capture of phosphate from wastewater by a recyclable ionic liquid functionalized polyacrylonitrile fiber: a typical "release and catch" mechanism. Environmental Science. Water Research & Technology, 2022, 8(3): 607–618
23. Shi X L, Du M, Sun B, Liu S, Jiang L, Hu Q, Gong H, Xu G, Liu B. A novel fiber-supported superbase catalyst in the spinning basket reactor for cleaner chemical fixation of CO_2 with 2-aminobenzonitriles in water. Chemical Engineering Journal, 2022, 430: 133204
24. Zhu H, Xu G, Du H, Zhang C, Ma N, Zhang W. Prolinamide functionalized polyacrylonitrile fiber with tunable linker length and surface microenvironment as efficient catalyst for Knoevenagel condensation and related multicomponent tandem reactions. Journal of Catalysis, 2019, 374: 217–229
25. Li T, Chen S, Li H, Li Q, Wu L. Preparation of an ion-imprinted fiber for the selective removal of Cu^{2+}. Langmuir, 2011, 27(11): 6753–6758
26. Shen J, Cao F, Liu S, Wang C, Chen R, Chen K. Effective and selective adsorption of uranyl ions by porous polyethylenimine-functionalized carboxylated chitosan/oxidized activated charcoal composite. Frontiers of Chemical Science and Engineering, 2021, 16(3): 408–419
27. Yang F, Huang J, Deng L, Zhang Y, Dang G, Shao L. Hydrophilic modification of poly(aryl sulfone) membrane materials toward highly-efficient environmental remediation. Frontiers of Chemical Science and Engineering, 2021, 16(5): 614–633
28. Xu G, Xu W, Tian S, Zheng W, Yang T, Wu Y, Xiong Q, Kianpoor Kalkhajeh Y, Gao H. Enhanced phosphate removal from wastewater by recyclable fiber supported quaternary ammonium salts: highlighting the role of surface polarity. Chemical Engineering Journal, 2021, 416: 127889
29. Xu G, Jin M, Wang F, Kalkhajeh Y K, Xiong Q, Zhang L, Tao M, Gao H. Construction of a phosphate-rich polyacrylonitrile fiber surface microenvironment for efficient purification of crystal violet wastewater. RSC Advances, 2019, 9(64): 37630–37641
30. Xu G, Wang L, Xie Y, Tao M, Zhang W. Highly selective and efficient adsorption of Hg^{2+} by a recyclable aminophosphonic acid functionalized polyacrylonitrile fiber. Journal of Hazardous Materials, 2018, 344: 679–688
31. Awual M R, Jyo A, El-Safty S A, Tamada M, Seko N. A weak-base fibrous anion exchanger effective for rapid phosphate removal from water. Journal of Hazardous Materials, 2011, 188(1−3): 164–171
32. Awual M R, Shenashen M A, Jyo A, Shiwaku H, Yaita T. Preparing of novel fibrous ligand exchange adsorbent for rapid column-mode trace phosphate removal from water. Journal of Industrial and Engineering Chemistry, 2014, 20(5): 2840–2847
33. Cui Z, Yang J, Chen W, Zhang S. Dyeing fine denier polypropylene fibers with phenylazo-*β*-naphthol-containing sulfonamide disperse dyes. Frontiers of Chemical Engineering in China, 2009, 4(3): 328–335
34. Zhang H, Fang D, Kong Z, Wei J, Wu X, Shen S, Cui W, Zhu Y. Enhanced adsorption of phthalic acid esters (PAEs) from aqueous solution by alkylbenzene-functionalized polypropylene nonwoven and its adsorption mechanism insight. Chemical Engineering Journal, 2018, 331: 406–415
35. Du J, Tao M, Zhang W. Fiber-supported acid-base bifunctional catalysts for efficient nucleophilic addition in water. ACS Sustainable Chemistry & Engineering, 2016, 4(8): 4296–4304
36. Shi X L, Zhang M, Li Y, Zhang W. Polypropylene fiber supported ionic liquids for the conversion of fructose to 5-hydroxymethylfurfural under mild conditions. Green Chemistry, 2013, 15(12): 3438–3445
37. Rahman S S, Siddiqua S, Cherian C. Sustainable applications of textile waste fiber in the construction and geotechnical industries: a retrospect. Cleaner Engineering and Technology, 2022, 6: 100420
38. Yousef S, Tatariants M, Tichonovas M, Kliucininkas L, Lukošiūtė S I, Yan L. Sustainable green technology for recovery of cotton fibers and polyester from textile waste. Journal of Cleaner Production, 2020, 254: 120078
39. Li F, Chen C, Wang Y, Li W, Zhou G, Zhang H, Zhang J, Wang J. Activated carbon-hybridized and amine-modified polyacrylonitrile nanofibers toward ultrahigh and recyclable metal

ion and dye adsorption from wastewater. Frontiers of Chemical Science and Engineering, 2021, 15(4): 984–997

40. Xu G, Xie Y, Cao J, Tao M, Zhang W Q. Highly selective and efficient chelating fiber functionalized by bis(2-pyridylmethyl)amino group for heavy metal ions. Polymer Chemistry, 2016, 7(23): 3874–3883
41. Luo Z, Guo M, Jiang H, Geng W, Wei W, Lian Z. Plasma polymerization mediated construction of surface ion-imprinted polypropylene fibers for the selective adsorption of Cr(VI). Reactive & Functional Polymers, 2020, 150: 104552
42. Zhang J, Shen Z, Mei Z, Li S, Wang W. Removal of phosphate by Fe-coordinated amino-functionalized 3D mesoporous silicates hybrid materials. Journal of Environmental Sciences, 2011, 23(2): 199–205
43. Cheng Y, He P, Dong F, Nie X, Ding C, Wang S, Zhang Y, Liu H, Zhou S. Polyamine and amidoxime groups modified bifunctional polyacrylonitrile-based ion exchange fibers for highly efficient extraction of U(VI) from real uranium mine water. Chemical Engineering Journal, 2019, 367: 198–207
44. Zhou X, Wei J, Zhang H, Liu K, Wang H. Adsorption of phthalic acid esters (PAEs) by amphiphilic polypropylene nonwoven from aqueous solution: the study of hydrophilic and hydrophobic microdomain. Journal of Hazardous Materials, 2014, 273: 61–69
45. Liu X, Ao J, Yang X, Ling C, Zhang B, Wang Z, Yu M, Shen R, Ma H, Li J. Green and efficient synthesis of an adsorbent fiber by preirradiation-induced grafting of PDMAEMA and its Au(III) adsorption and reduction performance. Journal of Applied Polymer Science, 2017, 134(25): 44955
46. Nataraj S K, Kim B H, dela Cruz M, Ferraris J, Aminabhavi T M, Yang K S. Free standing thin webs of porous carbon nanofibers of polyacrylonitrile containing iron-oxide by electrospinning. Materials Letters, 2009, 63(2): 218–220
47. Kavaklı C, Barsbay M, Tilki S, Güven O, Kavaklı P A. Activation of polyethylene/polypropylene nonwoven fabric by radiation-induced grafting for the removal of Cr(VI) from aqueous solutions. Water, Air, and Soil Pollution, 2016, 227(12): 473
48. Fung K L, Li R K Y, Tjong S C. Interface modification on the properties of sisal fiber-reinforced polypropylene composites. Journal of Applied Polymer Science, 2002, 85(1): 169–176
49. Ajmal Z, Muhmood A, Usman M, Kizito S, Lu J, Dong R, Wu S. Phosphate removal from aqueous solution using iron oxides: adsorption, desorption and regeneration characteristics. Journal of Colloid and Interface Science, 2018, 528: 145–155
50. Kamel R M, Shahat A, Hegazy W H, Khodier E M, Awual M R. Efficient toxic nitrite monitoring and removal from aqueous media with ligand based conjugate materials. Journal of Molecular Liquids, 2019, 285: 20–26
51. Sun X, Zhou Y, Zheng X. Comparison of adsorption behaviors of Fe-La oxides co-loaded MgO nanosheets for the removal of methyl orange and phosphate in single and binary systems. Journal of Environmental Chemical Engineering, 2020, 8(5): 104252
52. Awual M R, Hasan M M, Islam A, Rahman M M, Asiri A M, Khaleque M A, Sheikh M C. Introducing an amine functionalized novel conjugate material for toxic nitrite detection and adsorption from wastewater. Journal of Cleaner Production, 2019, 228: 778–785
53. Kumar P S, Korving L, van Loosdrecht M C M, Witkamp G J. Adsorption as a technology to achieve ultra-low concentrations of phosphate: research gaps and economic analysis. Water Research X, 2019, 4: 100029
54. Shan X, Zhao Y, Bo S, Yang L, Xiao Z, An Q, Zhai S. Magnetic aminated lignin/CeO_2/Fe_3O_4 composites with tailored interfacial chemistry and affinity for selective phosphate removal. Science of the Total Environment, 2021, 796: 148984
55. Zhang R, Leiviskä T, Taskila S, Tanskanen J. Iron-loaded Sphagnum moss extract residue for phosphate removal. Journal of Environmental Management, 2018, 218: 271–279
56. Zhao Y, Shan X, An Q, Xiao Z, Zhai S. Interfacial integration of zirconium components with amino-modified lignin for selective and efficient phosphate capture. Chemical Engineering Journal, 2020, 398: 125561
57. Zhang S, Zhang Y, Ding J, Zhang Z, Gao C, Halimi M, Demey H, Yang Z, Yang W. High phosphate removal using $La(OH)_3$ loaded chitosan based composites and mechanistic study. Journal of Environmental Sciences, 2021, 106: 105–115
58. Han C, Lalley J, Iyanna N, Nadagouda M N. Removal of phosphate using calcium and magnesium-modified iron-based adsorbents. Materials Chemistry and Physics, 2017, 198: 115–124
59. Almeida P V, Santos A F, Lopes D V, Gando-Ferreira L M, Quina M J. Novel adsorbents based on eggshell functionalized with iron oxyhydroxide for phosphorus removal from liquid effluents. Journal of Water Process Engineering, 2020, 36: 101248
60. Gamshadzehi E, Nassiri M, Ershadifar H. One-pot synthesis of microporous Fe_2O_3/g-C_3N_4 and its application for efficient removal of phosphate from sewage and polluted seawater. Colloids and Surfaces A: Physicochemical and Engineering Aspects, 2019, 567: 7–15